NEW MEXICO STATE UNIVERSITY
LAS CRUCES, NEW MEXICO

NASA CR 101689

ADVANCED STUDY OF VIDEO SIGNAL PROCESSING IN LOW SIGNAL TO NOISE ENVIRONMENTS

1967 - 1968

By

Frank Carden
Louis Corl

A Semi-Annual Progress Report

Submitted to

NATIONAL AERONAUTICAL SPACE ADMINISTRATION
WASHINGTON D. C.

NASA RESEARCH GRANT NGR-32-003-037

Electrical Engineering Department
Communication Research Group

May 1969

ENGINEERING EXPERIMENT STATION

NEW
MEXICO
STATE
UNIVERSITY
LAS CRUCES, NEW MEXICO

ADVANCED STUDY OF VIDEO SIGNAL PROCESSING IN LOW SIGNAL TO NOISE ENVIRONMENTS

1967 - 1968

By

Frank Carden
Louis Corl

A Semi-Annual Progress Report

Submitted to

NATIONAL AERONAUTICAL SPACE ADMINISTRATION
WASHINGTON D. C.

NASA RESEARCH GRANT NGR-32-003-037

Electrical Engineering Department
Communication Research Group

May 1969

ENGINEERING
EXPERIMENT
STATION

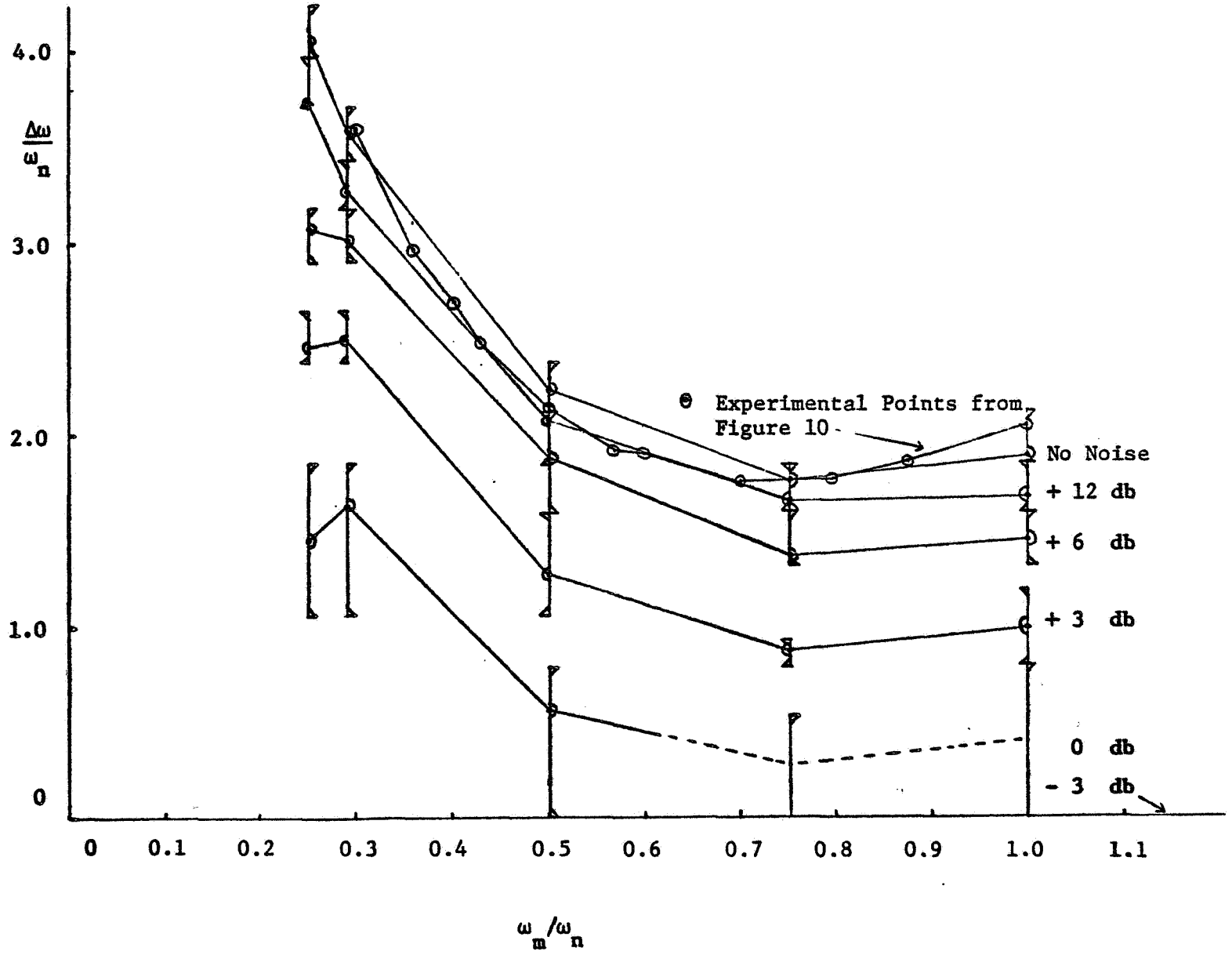
4.0
3.0
2.0
1.0
0
$\frac{\Delta\omega}{\omega_n}$
0
0.1
0.2
0.3
0.4
0.5
0.6
0.7
0.8
0.9
1.0
1.1
ω_m/ω_n
Experimental Points from Figure 10
No Noise
+ 12 db
+ 6 db
+ 3 db
0 db
- 3 db

ABSTRACT

This work is concerned with establishing a parameter space for acceptable operation of a PLL in a low signal to noise environment. An analog simulation of the IF model was used to establish and partition the parameter region into areas of acceptable operation. The input carrier to noise ratio determines the parameter of operation.

Table of Contents

List of Figures

List of Tables

CHAPTER I

CHARACTERIZING A PHASE-LOCK LOOP

A general phase-lock loop is diagrammed in Figure 1.

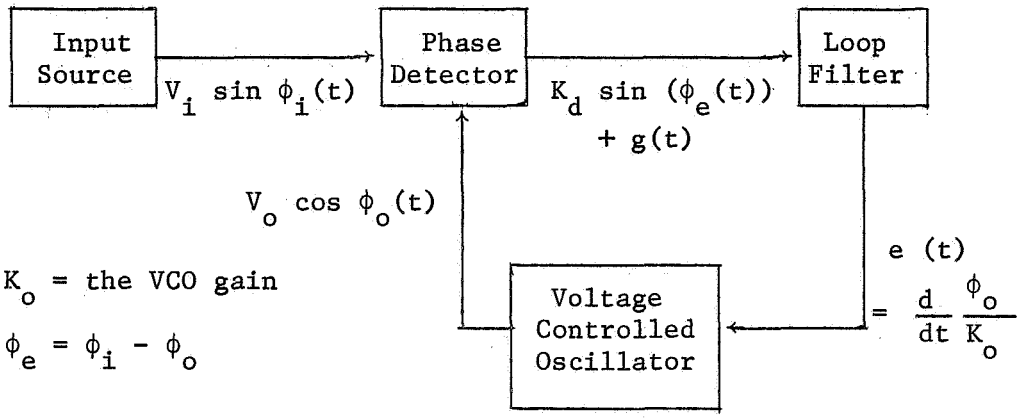

Figure 1
A General Phase-Lock Loop

The loop filter is chosen to determine the behavior of the loop. The loop filter that was used in the subsequent work had a transfer function $K_f(1+a/s)$. The loop with this filter is called a second order low pass loop by Gardner.[1]

A voltage controlled oscillator, VCO, produces a constant amplitude sinusoidal output whose instantaneous frequency is a linear function of the input voltage, e(t). That is, if $V_o \cos \phi_o(t)$ is the output then,

$$\frac{d}{dt} \phi_o = K_o \, e(t)$$

$$\phi_o(t) = K_o \int e(t) \, dt + K$$

Laplace transforming the first equation gives,

$$s\,\Phi_o(s) = K_o\,E(s)$$

$$\text{if } \phi_o(0) = 0$$

$$\Phi_o(s)/E(s) = K_o s^{-1}$$

This is the transfer function used to characterize the VCO.

The phase detector used was a product device, so

$$K_d \sin \phi_e(t) + g(t) = V_i \sin \phi_i(t)\; V_o \cos \phi_o(t)$$

$$= \frac{V_i V_o}{2} \sin\,[\phi_i(t) - \phi_o(t)] + \frac{V_i V_o}{2} \sin\,(\phi_i + \phi_o)$$

$$\text{Or } K_d = \frac{V_i V_o}{2} \text{ and } g(t) = \frac{V_i V_o}{2} \sin\,(\phi_i(t) + \phi_o(t))$$

Ordinarily in the analysis of the loop g(t) is neglected after arguing that its frequency is so high that the loop rejects it.

$$\phi_i(t) = \omega_c t + \theta_i(t)$$

$$\phi_o(t) = \omega_c t + \theta_o(t)$$

$$\phi_i(t) + \phi_o(t) = 2\omega_c t + \theta_i(t) + \theta_o(t)$$

This argument is true even though the loop filter in this case does nothing to reject high frequencies, since the VCO rejects high frequencies at e(t) with the characteristics of an integrator. The fact that the loop filter does not reject g(t) means that in a real loop either a filter must be put into the loop before e(t) or a filter must

be used on e(t) outside of the loop to reject g(t).

The action of the loop can now be diagrammed as shown in Figure 2 if g(t) is ignored.

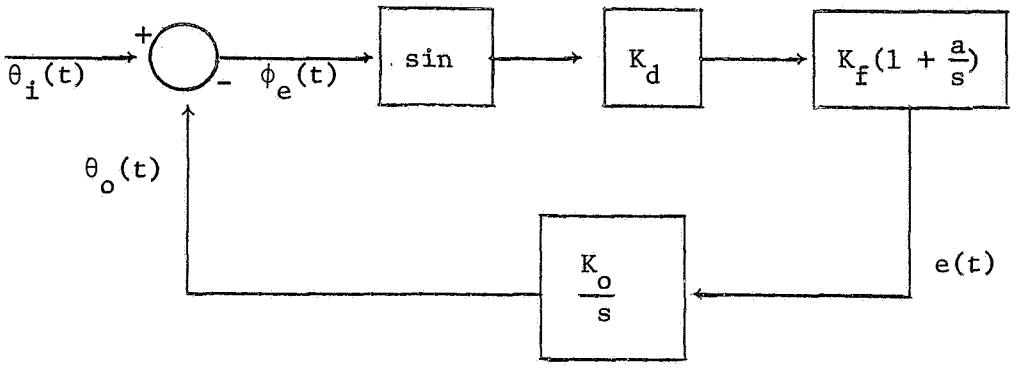

Figure 2
The Baseband Loop Model

If $\phi_e(t)$ is assumed small then a linear approximation that $\sin \phi_e(t) \simeq \phi_e(t)$ can be made to enable a transfer function to be written for the loop near lock.

This transfer function is,

$$\frac{\Theta_o(s)}{\Theta_i(s)} = \frac{K_o K_d K_f (1 + \frac{a}{s})(\frac{1}{s})}{1 + K_o K_d K_f (1 + \frac{a}{s})(\frac{1}{s})} = \frac{K_o K_d K_f (s + a)}{s^2 + K_o K_d K_f s + K_o K_d K_f a}$$

This is clearly a second order system with,

$$\omega_n^2 = K_o K_d K_f a \ , \quad \omega_n = \sqrt{K_o K_d K_f a}$$

and $2\zeta\omega_n = K_o K_d K_f$

$$\text{or} \quad \zeta = \frac{K_o K_d K_f}{2\sqrt{K_o K_d K_f a}} = 1/2 \sqrt{\frac{K_o K_d K_f}{a}} = \frac{\omega_n^2}{2\omega_n a} = \frac{\omega_n}{2a}$$

This second order system has a root locus as shown in Figure 3.

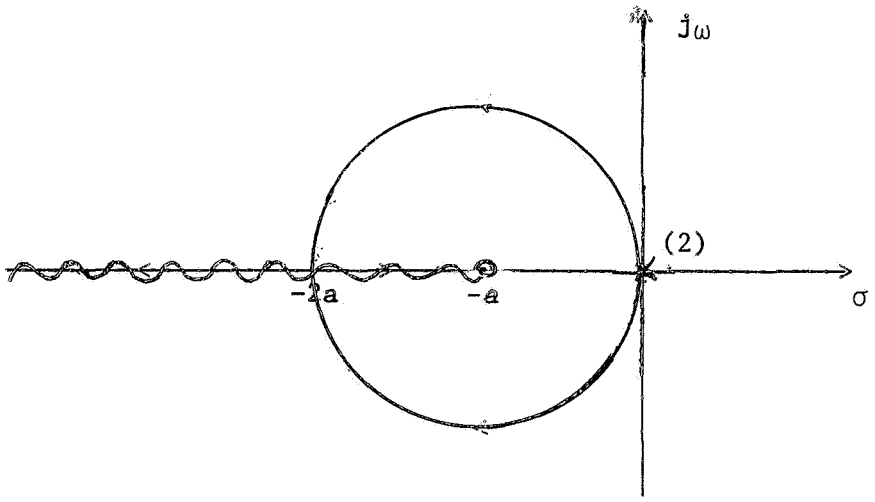

Figure 3
The Second Order, Low Pass Loop Root Locus

For a ζ of .707 the poles are at s = -a+ja and -a-ja.

It was an assumption throughout the following work that the second order phase-lock loop is completely characterized, even in its nonlinear behavior, by the two numbers ζ and ω. This was assumed true no matter what the values of K_o, K_d, and K_f as long as the product $K_o K_d K_f$ was unchanged.

The shape of the root locus for values of loop gain both greater and smaller than the static case should be very important in determining the nonlinear behavior of the loop. For instance, referring to Figure 2

on page 3, it is reasonable to expect that the loop gain is effectively decreased as ϕ_e approaches $\frac{\pi}{2}$ and that the small signal gain changes sign when ϕ_e is between $\frac{\pi}{2}$ and $\frac{3\pi}{2}$. For $\phi_e > \pi$ the loop would be expected to be unstable. In addition, amplitude modulation of the input carrier, by noise, for instance, can alter the loop gain in either direction. A noise phenomenon like IF impulses, which produce very low amplitude carrier input can thus be skipped over by a slowly responding low gain loop.

In other words, any alteration of the loop which changes the shape of the root locus near the static, closed-loop poles, even though leaving these latter unmoved can be expected to produce changes in the non-linear response characteristics.

CHAPTER II

THE LOOP TO BE SIMULATED

The actual loop to be studied has the characteristics that are listed below in Table 1, along with the scaled parameters used in the simulation.

TABLE I

LOOP PARAMETERS

Parameter and Symbol	Problem Values	Analog Computer Model Value
Intermediate Frequency IF, ω_c	$2\pi \cdot 50 \frac{\text{megaradians}}{\text{sec}}$	$2\pi \cdot 100 \frac{\text{radians}}{\text{sec}}$
Linearized Loop Natural Frequency ω_n	$10.9 \frac{\text{megaradians}}{\text{sec}}$	$21.8 \frac{\text{radians}}{\text{sec}}$
Linearized Loop Damping Ratio ζ_n	.707	.707
VCO Gain, K_o	Not Known	$2\pi(120) \frac{\text{radians}}{\text{sec} \cdot \text{unit}}$
Detector Gain, K_d	Not Known	1/8 units
Loop Filter Gain $K_f = \frac{2\zeta_n \omega_n}{K_o K_d}$	Not Known	.3271
Loop Filter Zero $a = \frac{\omega_n}{2\zeta_n}$	$\frac{10.9}{\sqrt{2}} \frac{\text{megaradians}}{\text{sec}}$	$15.41 \frac{\text{radians}}{\text{sec}}$

The computer model values were gotten by timescaling the problem with an α of 2×10^{-6} where

t = problem time

τ = computer time

$t = \alpha\tau$

This led to the computer scaled value of $\omega_c = 2\pi(100) \frac{\text{radians}}{\text{sec}}$ and $\omega_n = 21.8 \frac{\text{radians}}{\text{sec}}$. The value of α was chosen as a compromise between one giving higher frequencies, where the analog components would have been less accurate, and one giving lower frequencies, where the natural frequency of the loop would have restricted the modulation frequencies to a range even smaller than the 0 to 3.5 Hz of this particular simulation.

The unknown parameters of the problem were the VCO gain K_o, the detector gain K_d, and the loop filter gain K_f. The first one K_o, was chosen in the simulation both to give a VCO with a wide range of possible frequencies around 100 Hz, in fact, as high as 170 Hz without an overload, and to give accurate operation for small deviations around 100 Hz. The gain used to meet these conditions was $\frac{120 \text{ Hz}}{\text{unit}}$.

The next parameter, K_d, was chosen, as detailed below in the product detector description, to give the maximum output consistent with considerations of the maximum noise power to be present at some times in the later work. This value was 1/8 units which gave a signal $1/8 \sin \phi_e(t) + 1/8 \sin (2\omega_c t + \phi_i(t) + \phi_o(t))$ at the output when no noise was present.

Finally the third parameter, K_f, was chosen to produce a loop with $\zeta_n = .707$.

Since this value of K_f was

$$K_f = \frac{2\zeta_n \omega_n}{K_o K_d} \quad , \quad K_f = .3271$$

The product detector was simulated using a precision multiplier, EAI Model 7.127. This unit is a quarter square multiplier constructed to have a maximum error of 5 mv between 1/10 of the actual product of two input voltages, and the voltage observed at the output.

Since the output of the VCO is essentially a constant amplitude sinusoid, it was scaled to one unit peak value. The other input to the detector is the sum of an FM carrier and narrow band Gaussian noise. The carrier to noise power ratio was expected to get to 0 or -3 db, so the rms levels of the noise and carrier could be about equal. The likely maximum excursion of the noise is 3.5 times the rms level, so the carrier peak value was scaled to 1/4 of a unit. Then the rms level of the noise could be set as high as 1/3 unit with only a low probability of an overload.

$$1/4 + 3.5(1/3) \simeq 1.4 \text{ units for overload.}$$

This would give a carrier to noise power ratio of -6 db.

The output of the detector is d(t), the product of VCO output and carrier plus noise.

$$d(t) = \left[\frac{\cos(\omega_c t + \Theta_o)}{1} \right] \left[\frac{\sin(\omega_c t + \Theta_i)}{4} + n(t) \right]$$

$$= \left[\frac{\sin(\Theta_i - \Theta_o)}{8} \right] + \left[\frac{\sin(2\omega_c t + \Theta_i + \Theta_o)}{8} \right] + n(t) \left[\frac{\cos(\omega_c t + \Theta_o)}{1} \right]$$

The gain of the detector is thus $K_d = 1/8$ as defined by Gardner.[1]

The VCO was simulated by the implicit function generation technique.[2]

Writing,

$$\frac{d}{dt} \cos \Theta(t) = - \sin \Theta(t) \cdot \frac{d\Theta(t)}{dt}$$

$$\frac{d}{dt} \sin \Theta(t) = \cos \Theta(t) \cdot \frac{d\Theta(t)}{dt}$$

implies that network shown in Figure 4 will generate cos $\Theta(t)$ if $\dot{\Theta}(t)$ is supplied as the only input.

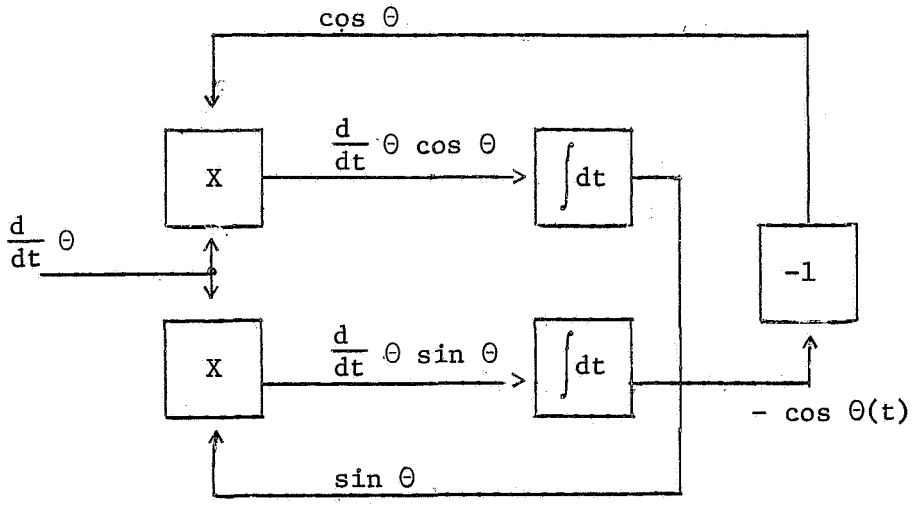

Figure 4

Implicit Function Generation of cos [$\phi(t)$]

This setup was constructed on the analog computer, but did not produce a constant amplitude output. Instead it appeared to have roughly an exponential decay or increase depending on the value of $\frac{d}{dt} \Theta(t) = \omega_c$ chosen for the test.

Since,

$$\frac{d}{dt}\left[e^{-At}\cos\Theta(t)\right] = -Ae^{-At}\cos\Theta(t) - e^{-At}\sin\Theta(t)\frac{d}{dt}\Theta(t)$$

$$= -\left[\frac{Ae^{-At}}{\dot{\Theta}(t)}\cos\Theta(t) + e^{-At}\sin\Theta(t)\right]\frac{d}{dt}\Theta(t)$$

And

$$\frac{d}{dt}\left[e^{-At}\sin\Theta(t)\right] = -Ae^{-At}\sin\Theta(t) + e^{-At}\cos\Theta(t)\frac{d}{dt}\Theta(t)$$

$$= -\left[\frac{Ae^{-At}}{\dot{\Theta}(t)}\sin\Theta(t) - e^{-At}\cos\Theta(t)\right]\frac{d}{dt}\Theta$$

It can be seen that an "A" small compared to $\frac{d}{dt}\Theta(t)$ represents a small phase shift in the loops. This phase shift probably occurs around the multipliers, since at 100 Hz the shift was positive and at 120 Hz or 40 Hz the shift was negative. That is, the implicit function generated is as shown in Figure 5 or 6.

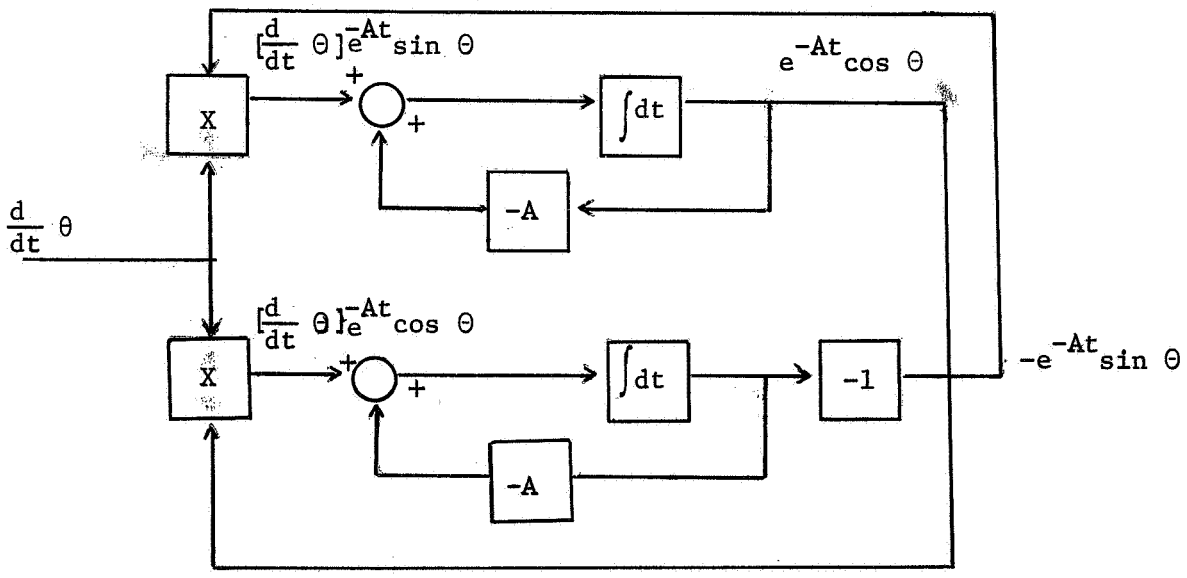

Figure 5

One View of the VCO Simulation Problem

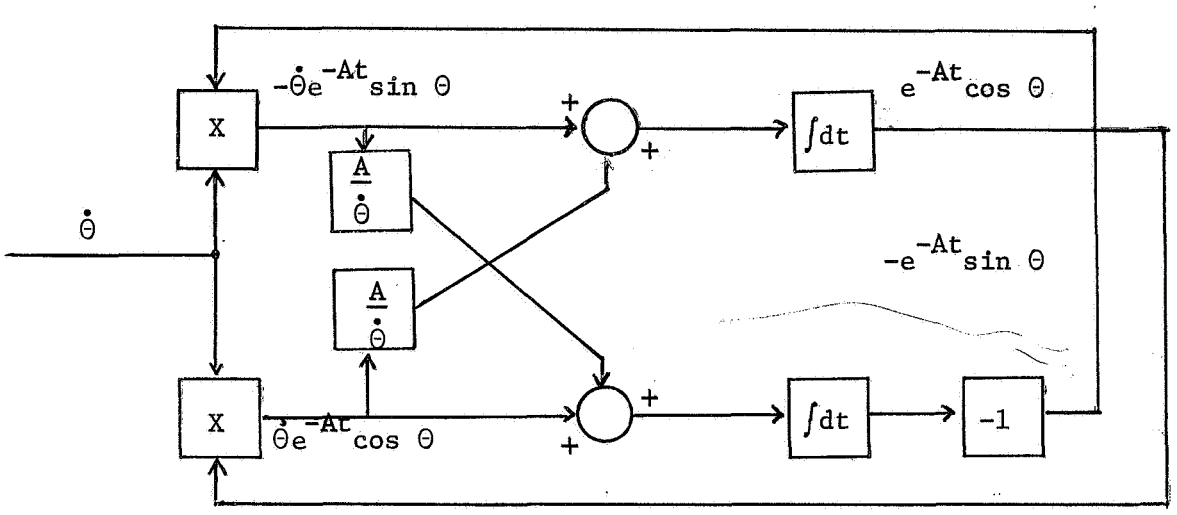

Figure 6

An Alternative View of Figure 5

In the second case, Figure 6, the indicated phase shifting for A>0 is such as to cause the multiplier outputs to lead their desired responses, i.e. A=0.

The first diagram above gives the best hint of the method used to stabilize the VCO performance. A positive feedback loop was inserted around an integrator to cancel the two negative feedback tendencies at all the desired operating frequencies. Then to eliminate the resulting exponential increasing tendency a limiter was added around the same integrator and set to limit the output to one unit peak value. The final computer diagram is shown in Figure 7 inside the VCO boundary.

The integrator gains were achieved either by running the TR-20 in the rep-op on, operate on mode or by bringing relay power to the front of the computer to be used to switch in the .02 μfd rep-op capacitor in the rep-op off modes.

When this VCO was constructed it was tested for constancy of output level as a function of frequency. The results were as shown in Table 2,

Table 2

VCO Output Level Variation With Frequency

Output Frequency (Hz)	Output Rms Level (units)
80	.7061
100	.7070
120	.7079

This data was sensitive to the amount of positive feedback set by pot 1, in Figure 7, having less variation in the level for larger settings of the pot. The output distortion, however, increased for larger settings, since the diode was biased on harder at the peak for more negative feedback.

The output distortion was measured with a HP Wave Analyzer (Model 302A). The results are in Table 3.

Table 3

VCO Output Harmonic Distortion

Output Frequency (Hz)	Harmonic	Voltage (db)
120	1	0
	2	-69
	3	-72
	4-10	-72
80	1	0
	2	-69
	3	-72
	4-10	-72

This data was taken at the VCO integrator with no feedback loops in Figure 7, since the output of the other was 7 db higher at the second harmonic.

The final question was the linearity of the VCO output frequency to input DC level. The readings in Table 4 were taken with $[\frac{d}{dt}\frac{\theta_o}{240\pi}]=0$ but with the loop otherwise as set up in Figure 7.

Table 4

VCO Gain Linearity

Input (units) (U_{in})	Output Observed (Hz)
.7000	82.871
.7600	89.985
.8200	97.059
.8800	104.18
.9400	111.30
.9993	118.33

These points are best fit by a line

$$f_{out} = (U_{in} - .8500)\ 118.50 + 100.616\ (Hz)$$

The VCO gain was in reality $2\pi(118.50)$, not $2\pi(120)$ as desired. This error was not found until the end of the research below, so the loop was one with $\zeta_n = .703$ instead of .707 and ω_n was also .6% low.

This 1.25% in the VCO gain was also observed at the $(\frac{\omega_c}{240\pi})$ pot in Figure 7. This pot had to be set at .8445 to cause the VCO to free run at 100 Hz. This level was set in the actual experiments, so there was no free running frequency error in the VCO, just in the small signal gain about that point. The cause of the error is not yet satisfactorily explained, although it also cropped up in the later attempt to build the IF bandlimiting filter. There the error was .5% low actual gains when the results were compared to the predictions.

The loop filter had a transfer function

$$\frac{E_o(s)}{E_i(s)} = K_f \left(1 + \frac{a}{s}\right) = .3271 \left(1 + \frac{15.41}{s}\right) \text{ for } f_n = 3.470 \text{ Hz}$$

This was simulated by the network shown in the Loop Filter boundary in Figure 7.

The loop was assembled from these three components as shown in Figure 7. After enough warmup time to stabilize the components, about 1/2 hour, the loop was adjusted as follows. The input carrier was set to 100 Hz and .1768 units [1/4(.7071)] rms with no modulation. The VCO output was set to .7071 units rms and the ω_c pot at the input to the VCO set to force the DC level of $e_o(t)$ to 0.000 units. Thus $e_o(t)$ becomes $\left[\frac{d}{dt}\frac{\Theta_o}{240\pi}\right]$. The loop so constituted acted in the manner predicted for a $\zeta_n = .707$, $\omega_n = 21.8 \frac{\text{radians}}{\text{sec}}$ loop when tested as discussed in the next chapter. This was true even though no additional provision was made for suppressing the second harmonic term of the phase detector output. This is also discussed in the following chapter. Here it is just argued that the VCO is itself a severe filter on any high frequency terms which attempt to propagate around the entire loop, so the presence of such terms at one point, [e(t)], should not be expected to effect the loop behavior.

The simulation of the phase-lock loop requires

a) Three multipliers, preferably high precision.
b) Three integrators, two with gains of 500 and 1000, and one with a gain of 2.
c) Twelve amplifiers.
d) Seven Pots.
e) One diode.

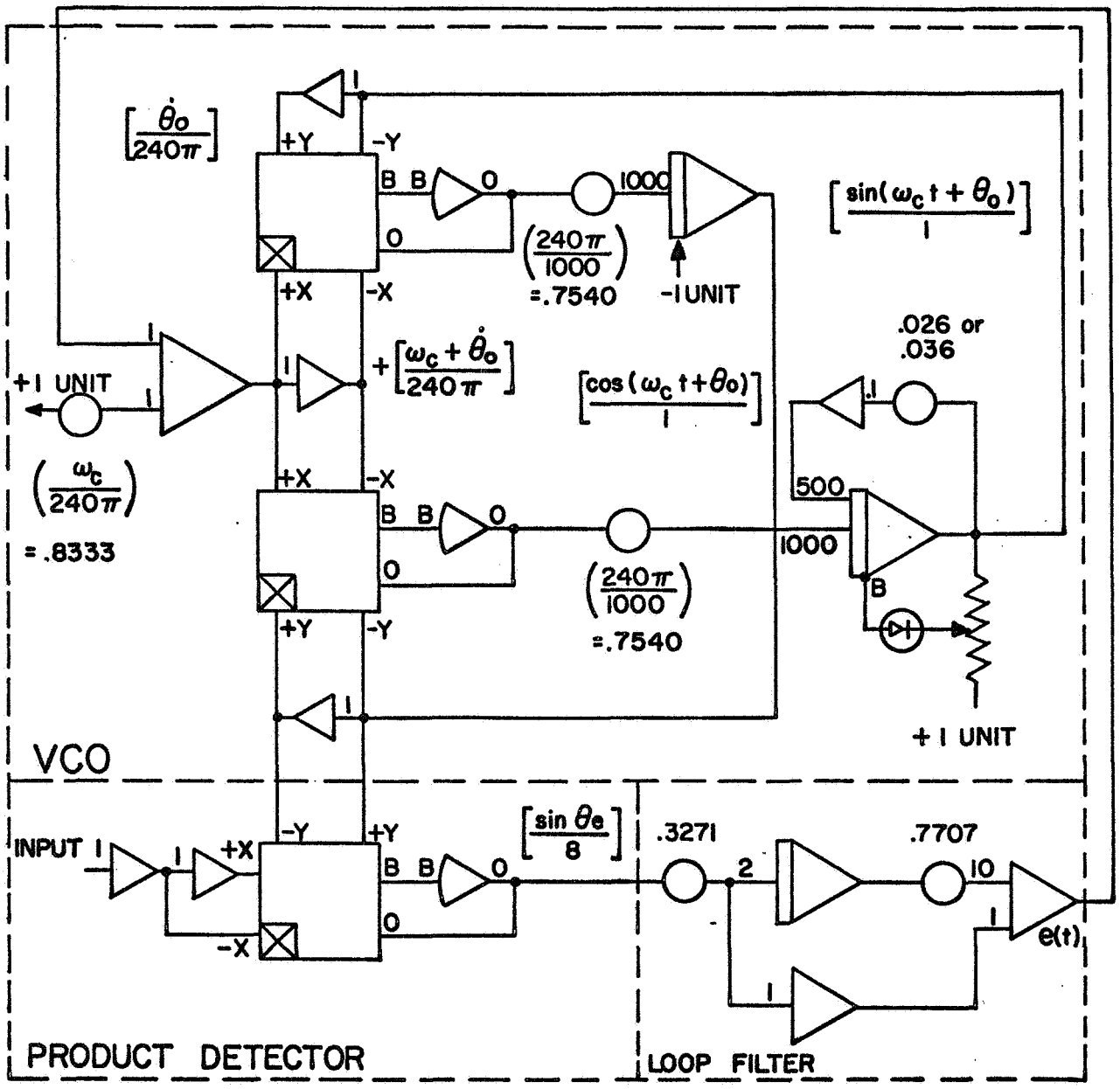

Figure 7

The Phase-Lock Loop Simulation

CHAPTER III
TESTS OF THE LOOP SIMULATION

This chapter presents tests conducted to determine if the loop constructed out of the three modeled elements discussed in the previous chapter acted in the manner predicted for such a loop. The results of these tests, while not conclusive, did suggest that the loop performed as predicted and showed that relatively minor alterations produced noticeable changes. Since that loop includes no component specifically designed to eliminate the second harmonic of the input some additional effort was expended looking at ways of doing this with minimal effect on the loop. In the end it was concluded that the loop functioned best without such filters included, so they were not used in the subsequent studies.

In the paper "The Quasi-Stationary and Transient Behavior of Non-Linear Phase-Lock Loops" by Carden, Lucky, and Swinson,[3] there is a study of the second order loop response to variable step changes in frequency. There is a prediction that a loop with $\zeta_n = .707$ will barely skip one cycle when $\frac{\Delta f}{f_n} = 3.09$ and two cycles when $\frac{\Delta f}{f_n} = 3.64$. These two numbers changed only slightly for $\zeta_n = .6$, where they are 2.88 and 3.41, or $\zeta_n = .8$, where they are 3.21 and 3.83, so this test is at best indicative and not definitive.

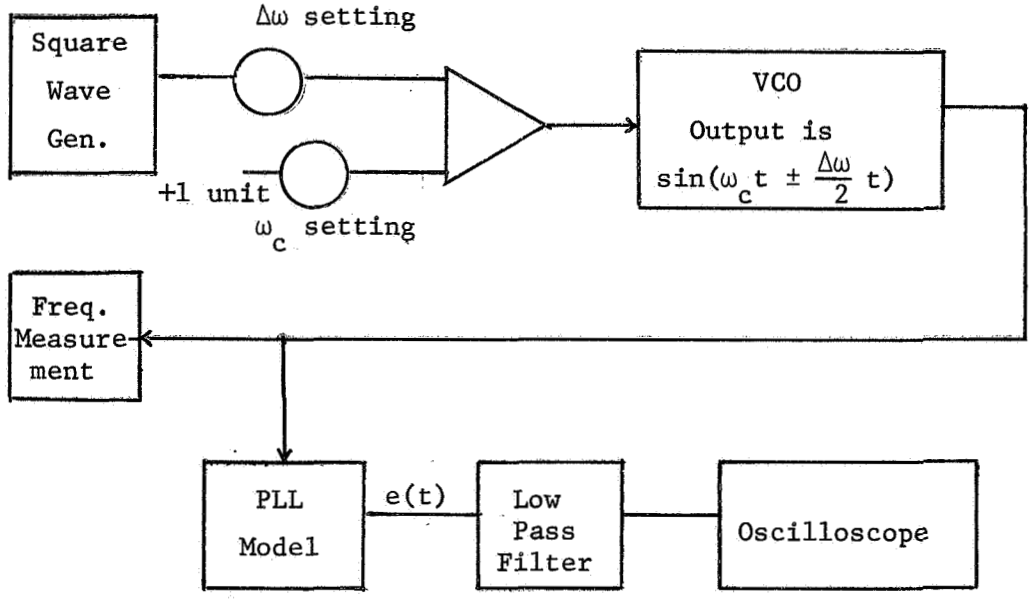

Figure 8

A Block Diagram of the Test Setup

Figure 8 shows the setup used for the following test. This test was performed by using two signal generators, one as a source of a very low frequency square wave which then frequency modulated the second around a free running frequency of 100 Hz. Both of these signal generators were Hewlett Packard 3300's. The square wave was slow enough that the loop transients had died out after one step change before the next step change occurred. Also ten periods of the loop input frequency could be counted at both the low and high frequencies. The loop signal e(t) was filtered to eliminate the second harmonic of the carrier and the resulting signal examined to determine when a cycle skip occurred. See Figure 9 and the associated discussion of this filter.

The following results were observed for the events listed assuming always that f_n was 3.470 Hz.

a) Just barely one cycle skip in going from a low to a high frequency only.

$$\frac{\Delta f}{f_n} = 3.03$$

b) Just barely one cycle skip in going from a high to a low frequency and one the other way.

$$\frac{\Delta f}{f_n} = 3.10$$

c) Just barely two cycle skips in going from a low to a high frequency and one the other way.

$$\frac{\Delta f}{f_n} = 3.52$$

d) Just barely two cycle skips in going from a high to a low frequency and two the other way.

$$\frac{\Delta f}{f_n} = 3.64$$

These results were repeatable to +.02 and they also did not depend on the starting or ending frequency more than +.02 for a shift of $\frac{\Delta f}{2}$. These anomalous results were in close agreement with those predicted when the cycle skipping occurred both directions.

Exactly what about the loop caused it to skip a cycle more easily in the low-to-high frequency direction was not investigated. The assumption was made that the cause of the asymmetry of the loop would not affect the results of any other experiments appreciably.

The results above showed that with no effort made to remove the second harmonic of the carrier from the loop, the loop behaved as a $\zeta_n = .707$, $f_n = 3.47$ Hz loop was predicted to by a model which eliminated the second harmonic, (the differential equation investigated by Carden, Lucky, and Swinson).

One attempt to eliminate the second harmonic used a filter of the form

$$F(s) = \frac{\omega_f^2}{s^2 + \omega_f s + \omega_f^2}$$

The modeling of this filter is shown in Figure 9.

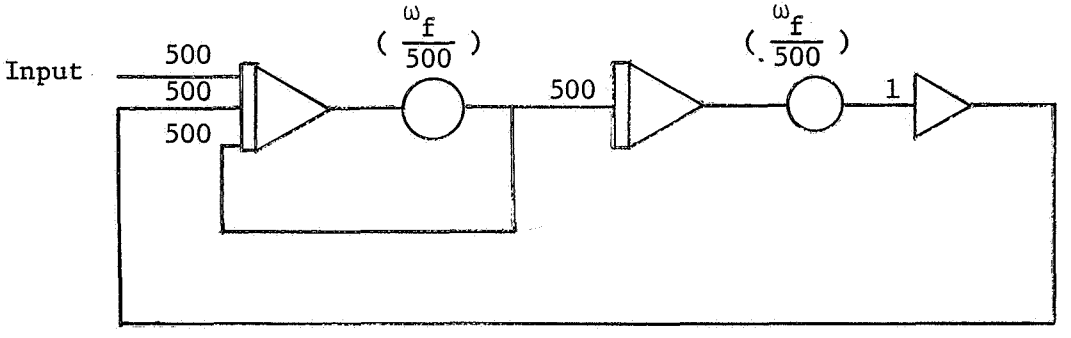

Figure 9

A General, Second Order, Low Pass Filter

This filter is approximately gain 1 out to $s = \omega_f$ and then drops at -40 db/dec. The parameter ω_f was set to be larger than ω_n of the loop, but much smaller than $2\omega_c$, the second harmonic of the carrier. A value of $\omega_f = 6.3\ \omega_n = \frac{2\omega_c}{8.5}$ was used to get the following results

on the test used above. Again $f_n = 3.470$ Hz.

a) One cycle skip low to high frequency only.

$$\frac{\Delta f}{f_n} = 2.90$$

b) One cycle skip high to low frequency and one the other way.

$$\frac{\Delta f}{f_n} = 2.91$$

c) Two cycle skips low to high frequency and one the other way.

$$\frac{\Delta f}{f_n} = 3.36$$

d) Two cycle skips high to low frequency and two the other way.

$$\frac{\Delta f}{f_n} = 3.41$$

These results are equivalent to $\zeta = .60$ for the assumed ω_n. Since the loop functioned better without a second harmonic filter internally connected, the next test was done without it, and it was never replaced.

The paper, "The FDM Demodulating Characteristics of Non-Linear Phase-Lock Loops" by Carden, Kelly and Hintz,[4] has a prediction of the maximum level of sinusoidal modulation at frequencies below ω_n on which the $\zeta_n = .707$ loop will remain locked without skipping cycles. The set up of Figure 8 was used again except that the modulation generator was switched over to sinusoidal output. Also the value of $\Delta\omega$ in the expression for the input signal

$$s(t) = A \sin \left(\omega_c t + \frac{\Delta\omega}{\omega_m} \sin \omega_m t\right)$$

could only be measured by monitoring the Hewlett Packard VCO input voltages and knowing the gain K_v of that VCO. Thus the counter on the

VCO output was not used any longer.

The procedure used was the following.

a) A modulation frequency was selected and $\Delta\omega$ level into the VCO decreased to zero.

b) The output of the phase-locked loop, e(t), was filtered through a low pass filter designed to eliminate the second harmonic of the carrier, but pass the modulation and a number of its harmonics. This was a second order filter with $\zeta = .5$ and corner frequency 2.5 ω_n or 5.1 ω_n. It attenuated 200 Hz at least 40 db below the input level. See Figure 9 for the model of this filter.

c) As the modulation level was increased the demodulated output at e(t) was watched in order to spot the first occurrence of a cycle skip. The level of modulation which caused this was measured and converted to $\Delta\omega$.

d) The procedure was repeated for another modulation frequency.

Following reference (4), the results were plotted on a graph, Figure 10, normalized as $\frac{\Delta\omega}{\omega_n}$ vs $\frac{\omega_m}{\omega_n}$. Also plotted is the curve $\Delta\omega\omega_m = \omega_n^2$ which was found in reference (3) to be an approximate boundary for stable locked operation. The results of the computer study from the other Carden paper are also plotted to verify the results of this loop simulation.

Because of the close agreement here as before it was assumed that the simulated loop was acting as a $\zeta = .707$, $\omega_n = 2\pi$ (3.47)loop should. Nothing is known, however, about the effect a change in the parameter ζ

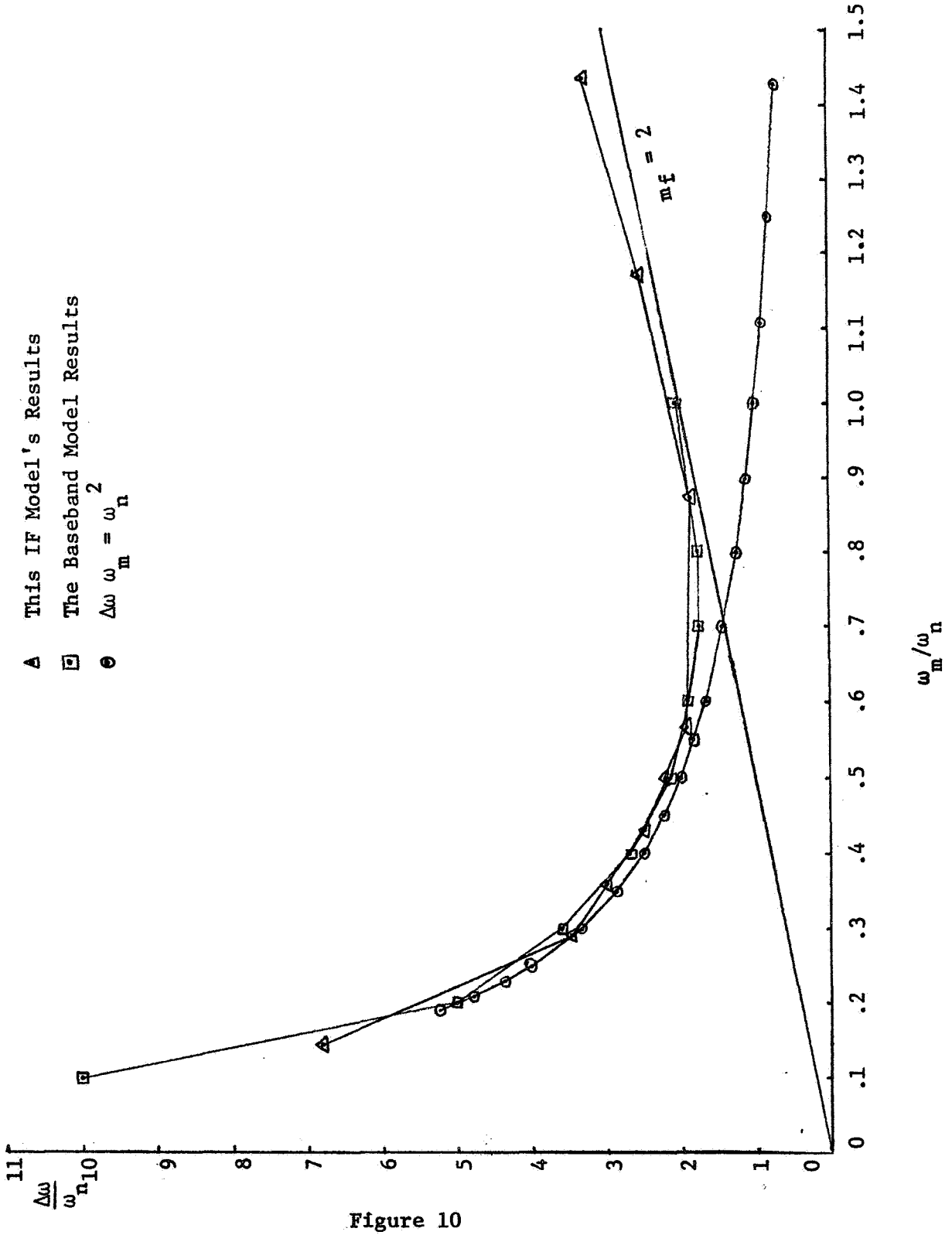

Figure 10

Loss of Lock on a Single Subcarrier

has on these results.

A second filter considered for use in the loop to eliminate the second harmonic of the input is the band rejection filter with transfer function

$$F(s) = \frac{s^2 + \omega^2}{s^2 + 2\zeta\omega s + \omega^2} = \frac{1 + \frac{\omega^2}{\omega^2}}{1 + \frac{2\zeta\omega}{s} + \frac{\omega^2}{s^2}}$$

The ζ of the pole has very little effect on the character of this filter, which is determined primarily by the zeroes at $s^2 = -\omega^2$. This filter was modeled as shown in Figure 11.

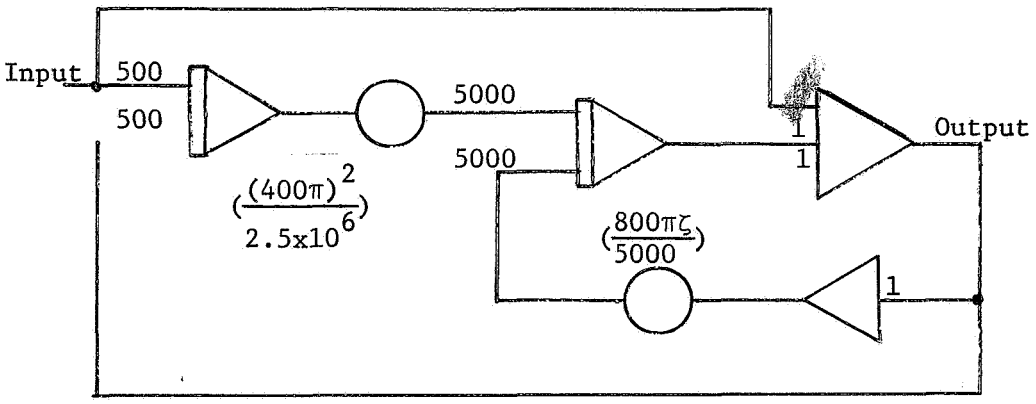

Figure 11

A Narrowband Rejection Filter

The zero was put at 200 Hz, the second harmonic of the input carrier. ζ was set to 1 because this gives the maximum attenuation by the poles while maximizing the frequencies of the poles. That is, for $\zeta \leq 1$ the poles are at a constant distance from the origin of the s plane, while

for $\zeta > 1$ one pole is closer and one farther away. This filter's frequency response was then measured and some of the results are in Table 5.

Table 5

Rejection Bandwidths of the Filter in Figure 11

Output attenuation (from 20 Hz set at 0 db)		Bandwidth
-15 db	169.3 Hz to 236.6 Hz	67.3 Hz
-20 db	182.3 Hz to 220.0 Hz	37.7 Hz
-25 db	189.9 Hz to 211.1 Hz	22.2 Hz
-30 db	194.3 Hz to 206.2 Hz	11.9 Hz
-35 db	197.1 Hz to 203.5 Hz	6.6 Hz

The results indicate that a signal with wide bandwidth will not be very greatly attenuated by the filter at its band edge. This is characteristic of the input carrier to this loop and also of the second harmonic signal which this filter is intended to suppress. For instance, when the behavior of the loop is being studied anywhere near the loss of lock curve in Figure 10, $\frac{\Delta\omega}{\omega_n}$ is greater than 2, while m_f is greater than 2. The bandwidth of the second harmonic signal is

$$W = \beta m_f f_m = \beta \Delta f \geq 4 f_n = 14 \text{ Hz}$$

Since $$2 \leq \beta \leq 4 \text{ for } m_f > 2$$

When $m_f = 2$ and $\omega_m = \omega_n$, W is 28 Hz. The attenuation of the band edge is thus not much more than -20 db and can be much less.

To investigate the above predictions the loop was set up and the signal e(t) was passed through this filter outside the loop. When the

values of $\Delta\omega$ and ω_m were set to give nearly unlocked operation, e(t) exhibited a large amount of second harmonic riding on the peaks. When e(t) is near zero, the second harmonic is nearly centered on the filter's zero, so it is heavily attenuated. At $\omega_m = .1\omega_n$ the attenuation of the second harmonic at the peak of e(t) was only -6 db from the input level. At $\omega_m = \omega_n$ the attenuation was better at about -26 db.

Since the conclusion here was that this filter did not help much, it was not put into the loop to see whether it, in fact, degrades the system any.

CHAPTER IV

THE GENERATION OF NARROWBAND NOISE

Once the loop had been satisfactorily simulated the effort turned to investigating its behavior in the presence of large amounts of narrowband noise added onto the input carrier. The Apollo Unified S-band specifications called for IF Bandwidths of 1, 2, 4, 14 MHz. A 4 MHz bandwidth was used in this work. In the absence of any clarifying statement these were considered to be equivalent-noise bandwidths, not 3 db bandwidths.

The equivalent-noise bandwidth is defined[5] as

$$W(Hz) = \frac{1/2\pi \int_0^\infty |H(j\omega)|^2 \, d\omega}{H_{max}^2}$$

This means that a square bandpass filter of width W and power gain H_{max}^2 passes the same power that the filter $H(j\omega)$ passes when the input is white noise in both cases.

Shown in Table 6 are some simple bandpass filters and their calculated $|H(j\omega)|$ max and W

Table 6

Equivalent - Noise Bandwidths

		$\lvert H(j\omega)\rvert_{max}$	W
1.	$H_1(s) = \frac{s}{s^2 + 2\zeta\omega_c s + \omega_c^2}$	$\frac{1}{2\zeta\omega_c}$	$\frac{\omega_c\zeta}{2}$
2.	$H_2(s) = \frac{s^2}{(s^2 + 2\zeta\omega_c s + \omega_c^2)^2}$	$\frac{1}{4\zeta^2\omega_c^2}$	$\frac{\omega_c\zeta}{4}$
3.	$H_3(s) = \frac{s^3}{(s^2 + 2\zeta\omega_c s + \omega_c^2)^3}$	$\frac{1}{8\zeta^3\omega_c^3}$	$\frac{3\omega_c\zeta}{16}$

An equivalent-noise bandwidth of .08 f_c requires that

$$\frac{.08\omega_c}{2\pi} = \frac{\omega_c\zeta}{4}$$

in the fourth order case, or

$$\zeta = \frac{.16}{\pi} = .051$$

The higher order filters are preferable, since they give squarer responses, but the improvement between fourth and sixth order filters is not great enough to warrant the trouble of building the third section. The filter simulation is shown in Figure 12 where ω_c is $2\cdot\pi\cdot100$ and $\zeta = .051$.

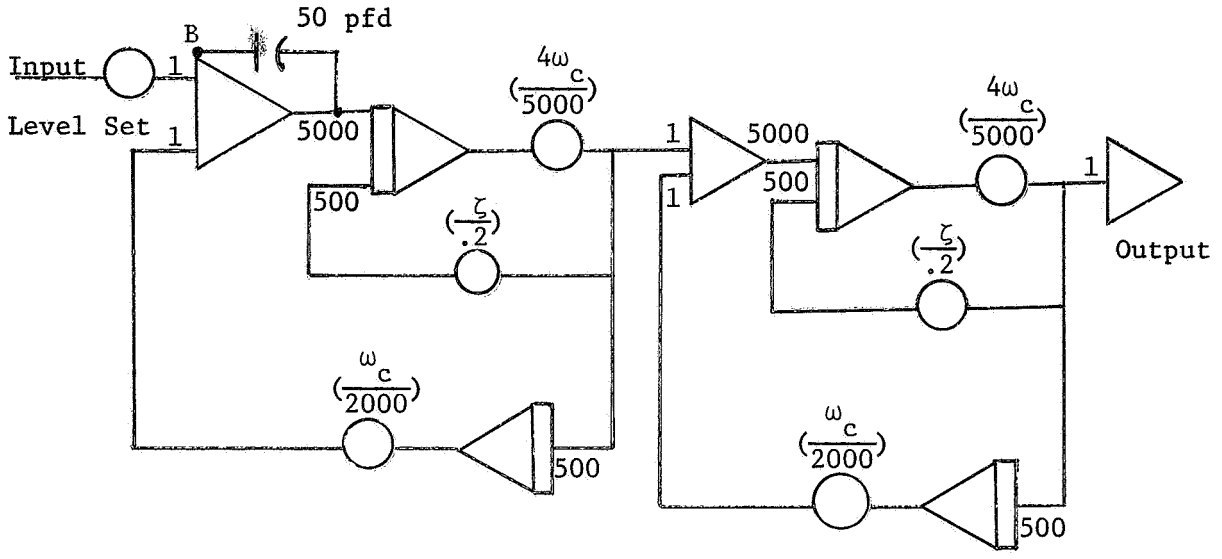

Figure 12

The IF Bandpass Filter

The input is broadband, Gaussian white noise of known spectral density. The output level is controlled with the setting of the input pot. The bypass capacitor of the first amplifier low pass filters the input to make the noise bandwidth less than the bandwidth of the amplifiers throughout the network. This kept the overload lights off until the output signal actually overloaded the last integrator on the largest excursions of the noise. The pole added by the capacitor was at about

$$\omega = \frac{1}{10^5\ \Omega \times 50 \times 10^{-12} \text{fd}} = 2 \times 10^5\ \frac{\text{radians}}{\text{sec}}$$

$$f \simeq 30\ \text{KHz}$$

Thus this pole has relatively little effect on the spectral density at 100 Hz, where the filter above was peaked.

A true rms voltmeter was put on the output to calibrate the input level pot. The output rms level was linear with respect to the setting of this pot, and the constant of proportionality was used to set power levels from then on. The output of the filter for no input was about 6mVrms, so the filter is not generating much noise on its own.

When this filter was first simulated it was noticed that the peak frequencies of the individual sections were at 99.5 Hz. When the two sections were connected in series the peak moved to 101.0 Hz. This was not taken as a sign of bad interaction and the pot values, $(\frac{4\omega_c}{5000})$ and $(\frac{\omega_c}{2000})$ were decreased by 1% to give a filter with a peak at 100 Hz. A plot of the pass character of the filter was made and the asymmetry of the results was ignored. Thus the filter simulation used in the subsequent studies was in fact quite poor. Only later was it found that the two sections, simulated on adjacent amplifiers with patch wires only millimeters apart in some cases, were strongly coupled near the peak.

This coupling produced an asymmetry of the pass character in addition to shifting the peak frequency the 1.5 Hz noticed above. If the polarity of the coupling was reversed by placing an inverter between the sections, the asymmetry switched from one side of the pass band to the other and the peak shifted 1.5 Hz in the other direction from 99.5 Hz. When this was discovered, the single section pass characters were measured and it was found that each one of them was very close to the predicted shape although peaked at 99.5 Hz instead of 100 Hz. Thus the major coupling was between sections and not internal to a single section.

Then the two sections were constructed on opposite sides of the patch board to minimize the coupling. This produced a fourth order filter with a symmetric pass character quite close to that predicted for a peak at 99.6 Hz. The equivalent-noise bandwidth was 7.9 Hz instead of 8.0 Hz. These results were taken to mean that the interstage coupling is not completely eliminated, but that it now only shifts the peak .1 Hz and produces no noticeable asymmetry.

The asymmetry of the first filter gave it an equivalent-noise bandwidth of 6.8 Hz. This means that the results from it are strictly applicable only to a 3.4 MHz IF bandwidth and not the 4 MHz intended. When the coupling was eliminated, the filter produced identical results to those before, if its equivalent noise bandwidth was set to 6.8 Hz.

The source of noise for this filter was an ELGENCO model 603A Gaussian white noise generator. The manual[6] said that the spectral density was $G_E = 1.1 \times 10^{-3} \frac{\text{Vrms}}{\sqrt{\text{Hz}}}$. There was also no explanation of what this spectral density meant.

Spectral density ordinarily has units of $\frac{(\text{Volts})^2}{\text{Hz}}$ and is called power spectral density when a one ohm load is assumed. Then the power out of a filter is

$$P = \frac{\overline{V^2}}{1\Omega} = 2 \int_o^\infty \frac{G(f)}{2\pi} |H(j\omega)|^2 \, d\omega$$

And if G(f) is constant

$$P = 2G\, H^2_{max} \left[1/2\pi \int_o^\infty \frac{|H(j\omega)|^2}{H^2_{max}} \, d\omega\right]$$

The term in parentheses is the equivalent-noise bandwidth of the filter in question, W.

$$P = \frac{\overline{V^2}}{1\Omega} = 2G\,H_{max}^{\,2}\,W$$

$$\overline{V} = (\sqrt{2G})\,(H_{max})\,(\sqrt{W})$$

Apparently the first factor on the right is what the ELGENCO manual gives as spectral density.

$$G_E = \sqrt{2G}$$

As evidence that this was indeed so, the noise generator was set to 1 Vrms out (the level at which it was assumed the spectral densities are to be measured) and fed into the band pass filter simulation. In the case of the filter with large internal coupling the maximum gain was 1700, the equivalent-noise bandwidth was 6.8 Hz, and the output was 5.1 Vrms/Vrms in

$$G_E = \frac{\overline{V}}{\sqrt{W}\;H_{max}} = \frac{5.1}{\sqrt{6.8}\;\;1700} = 1.15 \times 10^{-3}\,\frac{\text{Vrms}}{\sqrt{\text{Hz}}\;\;\text{Vrms in}}$$

In the case of the filter with small internal coupling, the maximum gain was 1585, the equivalent-noise bandwidth was 7.9 Hz, and the output was 5.0 Vrms/Vrms in

$$G_E = \frac{\overline{V}}{\sqrt{W}\;H_{max}} = \frac{5.0}{\sqrt{7.9}\;\;1585} = 1.12 \times 10^{-3}\,\frac{\text{Vrms}}{\sqrt{\text{Hz}}\;\text{Vrms in}}$$

This agreement is good enough to imply that the ELGENCO number is as postulated above.

The manual[6] on the noise generator says that there is a dynamic range 3.5 times the rms value in the amplifiers. To provide the same protection the output of the last integrator in the filter needs to be less than

$$x = \frac{14 \text{ Volts overload}}{3.5} = 4.0 \text{ Vrms}$$

This limits the output power to about 2 Vrms since the pot, $(\frac{4\omega_c}{5000})$, is about .5. This is more than enough to give a carrier to noise power ratio of 0 db and as much as -6 db could be gotten by taking the noise output directly from the last integrator.

CHAPTER V

THE DEMODULATION OF A NOISY FM CARRIER

The problem studied with this simulation was the frequency demodulation characteristics of this loop for low carrier to noise power ratios.

The general idea was to generate a curve for a specific carrier to noise power ratio that showed what $\Delta\omega$ and ω_m combinations gave "good demodulation" of a frequency modulated input, and what combinations produced "significant degradation" of the output. "Good demodulation" and "significant degradation" were not defined, part of the problem being to settle on some measurement of the output which would distinguish these two cases.

This was done after some preliminary consideration of alternative measurements and the results are presented later in this chapter. The other measurements considered were not rejected after study as being unsatisfactory, they were just not as immediately appealing as what was finally settled on.

The technique settled on was a measurement of total power at the output for various combinations of the parameters ω_m, $\Delta\omega$, and carrier to noise power ratio. This was initially motivated by the following considerations.

a) One source of possible degradation of the demodulated output for high $\Delta\omega$ is the non-linear behavior of the loop seen already for the case of modulated carrier with no noise. As the loop approaches loss of lock on the signal alone, noise might be expected to increase the

probability of this event and thus decrease the amount of demodulated signal power.

b) The phase-lock loop is a linear system for small $\Delta\omega$, so "good demodulation" might be defined as that region in which the loop remains to some degree linear.

c) The average output power of a linear system is the mean square output voltage into one ohm, or $\overline{P}$ is

$$\overline{P} = \overline{[s(t) + n(t)]^2} = \overline{s^2(t)} + \overline{n^2(t)} + \overline{2s(t)n(t)}$$

If the signal and noise are uncorrelated, the last term is zero, so

$$\overline{P} = \overline{s^2(t)} + \overline{n^2(t)}$$

Also in the linear system superposition gives a means for measuring both signal and noise separately, since n(t) is left unchanged if the signal is turned off and s(t) is not altered if the noise is turned off.

These considerations led to the following scheme for characterizing the demodulation performance of the loop.

a) Pick a carrier to noise power ratio and measure the output noise power in the absence of signal, that is, with $\Delta\omega = 0$.

b) Turn the noise off and pick a modulation frequency. Measure the output signal power at different levels of $\Delta\omega$, from $\Delta\omega = 0$ up to and even beyond the point where the loop has lost lock.

c) Now turn the noise on and measure output power as a function of $\Delta\omega$ in the same range as in Part b. The difference between the power measured here at a specific $\Delta\omega$ and the sum of the noise power from Part a

and the signal power for that $\Delta\omega$ from Part b, is a measure of the deviation of the loop from linear behavior.

d) Go to Part b with a new modulation frequency.

e) When all the modulation frequencies desired have been used, go to Part a with a new carrier to noise power ratio.

The output power was measured by actually measuring the mean squared output voltage and assuming a 1 Ω load. The demodulated signal from the loop, e(t) or $[\frac{d}{dt}\ \frac{\theta_o}{240\pi}]$, was first low pass filtered to reject the second harmonics of the carrier. This filtering was not done specifically to bandlimit the FM demodulator noise, so the corner frequency was put at 5.1 ω_n. When this frequency was shifted to 2.5 ω_n in one test with 0 db carrier to noise ratio, the output noise power remained constant. Thus the loop noise is limited to 2.5 ω_n or less and is included in the output power measurements of this study.

After passing through this filter e(t) was squared with a non-precision quarter square multiplier. This has definite draw backs as far as accuracy goes, but it could not be avoided. In order to accomodate voltages 3.5 times the rms value, the output must be able to range $(3.5)^2$ times the mean squared value or 12 1/4 to 1. Thus the mean squared output level must be kept below $\frac{1.4}{12.25}$ or about .11 units. The rms value must be less than .33 units into the multiplier.

The signal out of the multiplier was effectively time averaged by passing it through a 100 sec time constant simple low pass circuit as shown in Figure 13.

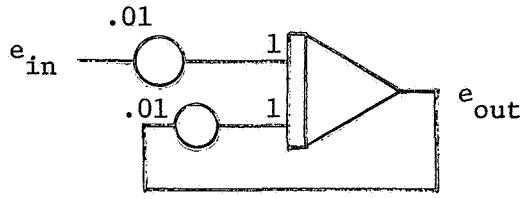

Figure 13
The Time Averaging Filter

For zero input this circuit had a -45 millivolt DC output. This was apparently due to the contact potentials of the pots.

This offset voltage was removed from all the data from this filter. The care taken in the use of the loop to remove the DC component of $\dot{\theta}_o$ by adjustment of the carrier and VCO frequency to equality was also important for getting good results from the mean square voltage measurements. The 100 sec time constant filter was not enough to smooth the output for easy reading, so after 500 secs of settling to a mean square level a 240 sec or 480 sec plot was made and the average value picked out by eye.

An alternative filter without the offset voltage of that in Figure 13 was the one shown in Figure 14.

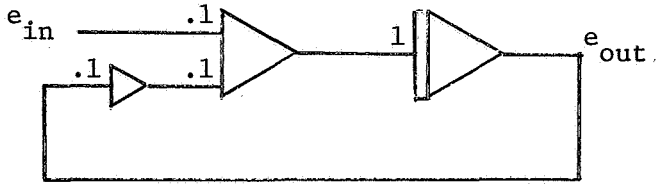

Figure 14

An Alternate Simulation of the Time Averaging Filter

It was also easier to set this filter to be accurately gain 1 or gain 10 at DC.

The setup used to collect the data was that shown in Figure 15.

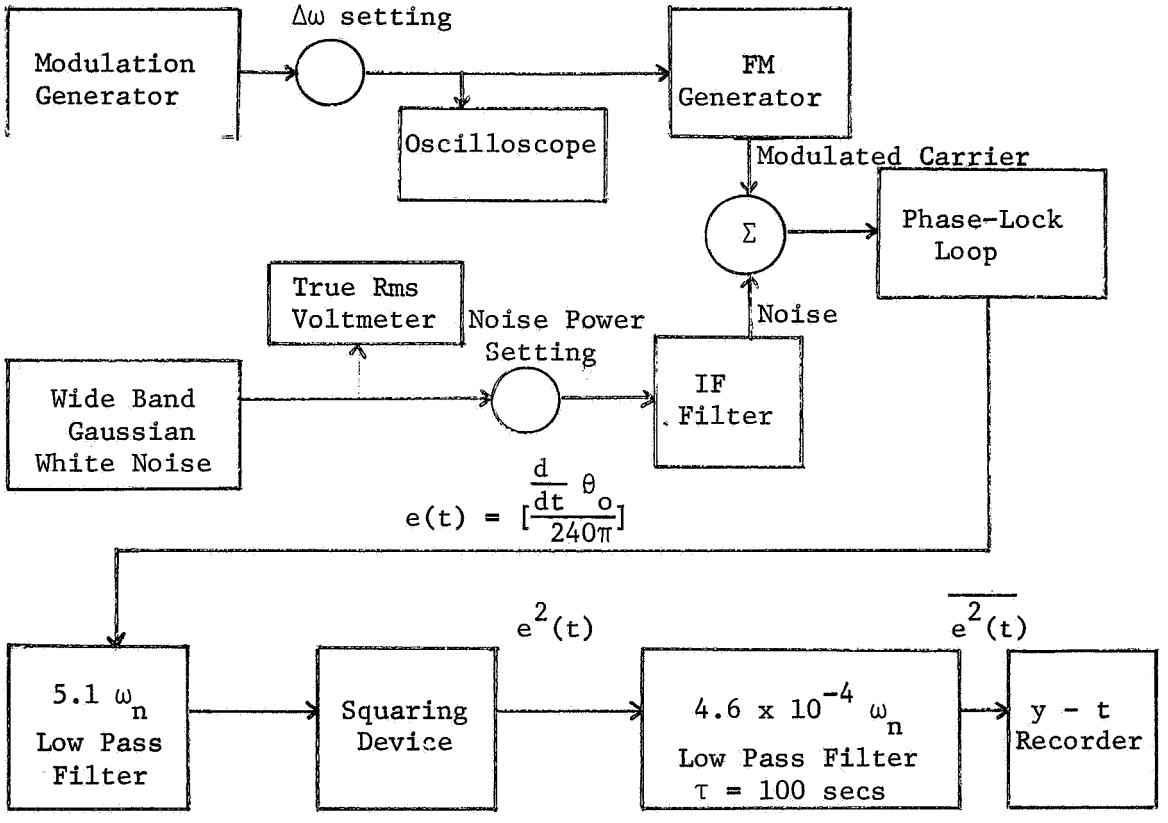

Figure 15
The Setup Used to Study Noisy Demodulation

Referring to Figure 15 the oscilloscope was used to measure the peak voltage set by the $\Delta\omega$ level control. This could then be converted to $\Delta\omega$. The true rms voltmeter was used to maintain the input noise level to 1 vrms within several per cent. This was better than the meter on the

front of the noise generator would allow and thus helped insure repeatability of the measurements. The noise power level control before the IF Filter was used to control the carrier to noise power ratio into the phase-lock loop.

The first observation made was that carrier to noise power ratios greater than 12 db were not very much different than the no noise case. Thus the values +12, +6, 3, and 0 db were settled on as the ones to study initially.

The second observation was that for the range of values given above, noise power out is directly proportional to noise power in. It is just below 0 db that this becomes no longer true. These results are displayed in Figure 16.

The third observation was that in the absence of noise, signal power out is directly proportional to signal power in up to the point where loss of lock occurs at each cycle. Because it is known that distortion appears in the demodulated signal before loss of lock, the same is not true of the power at the fundamental frequency, but the wide band low pass filter after e(t) passes at least the fifth harmonic and essentially all of the power. This fact was especially encouraging because it promised to make it relatively easy to tell when the signal power out in the presence of noise no longer followed signal power in as the linear analogy suggests it should.

The observations of the loop's behavior with both modulation and noise present are displayed in Figures 17 through 21. There is one for each of the five modulation frequencies studied, ω_n, $.75\omega_n$, $.5\omega_n$, $.25\omega_n$ and $.29\omega_n$ which was 1 Hz. The last was a convenient frequency

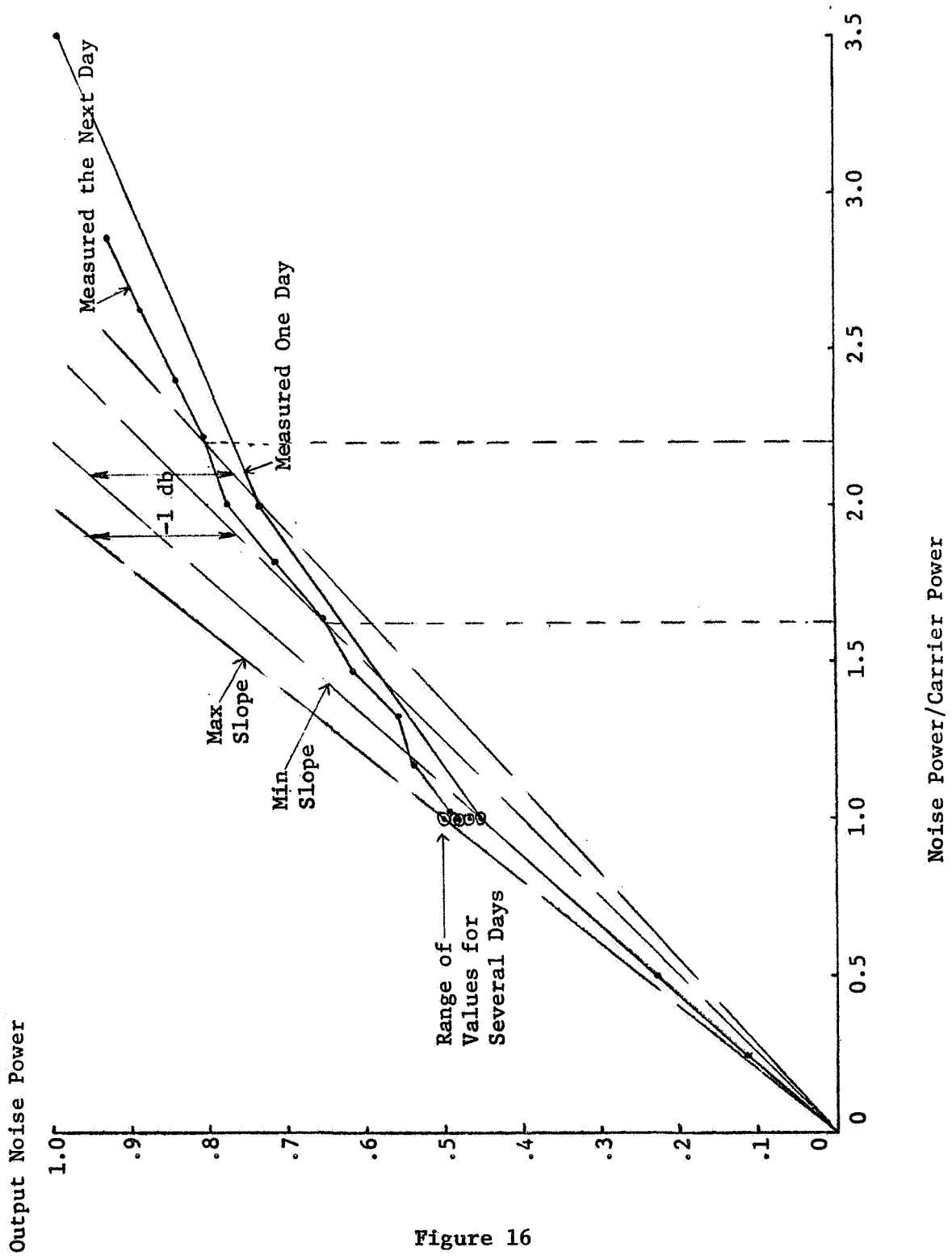

Figure 16

Output Noise Power vs. Input Noise Power

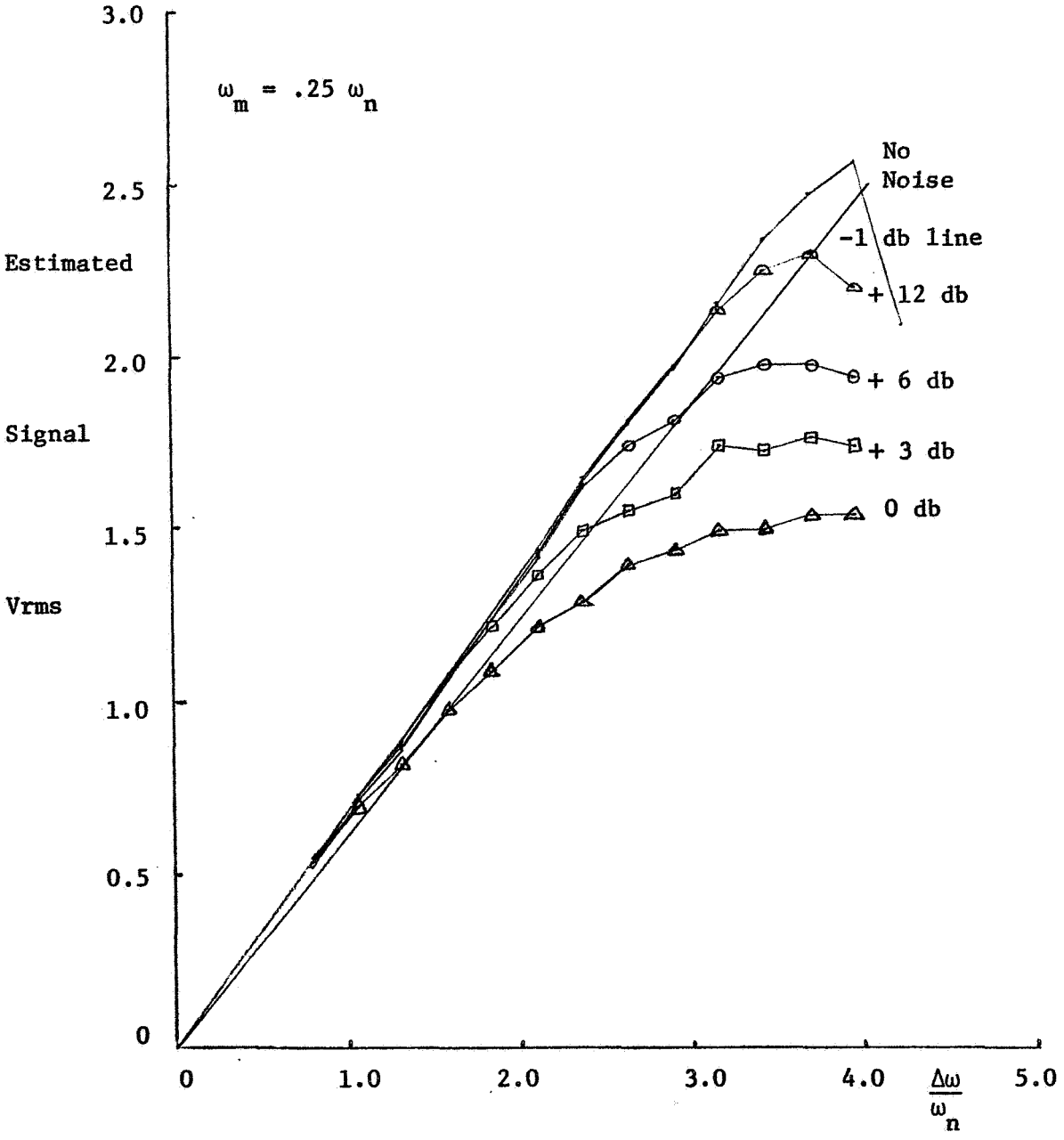

Figure 17

Estimated rms Signal vs. $\Delta\omega/\omega_n$

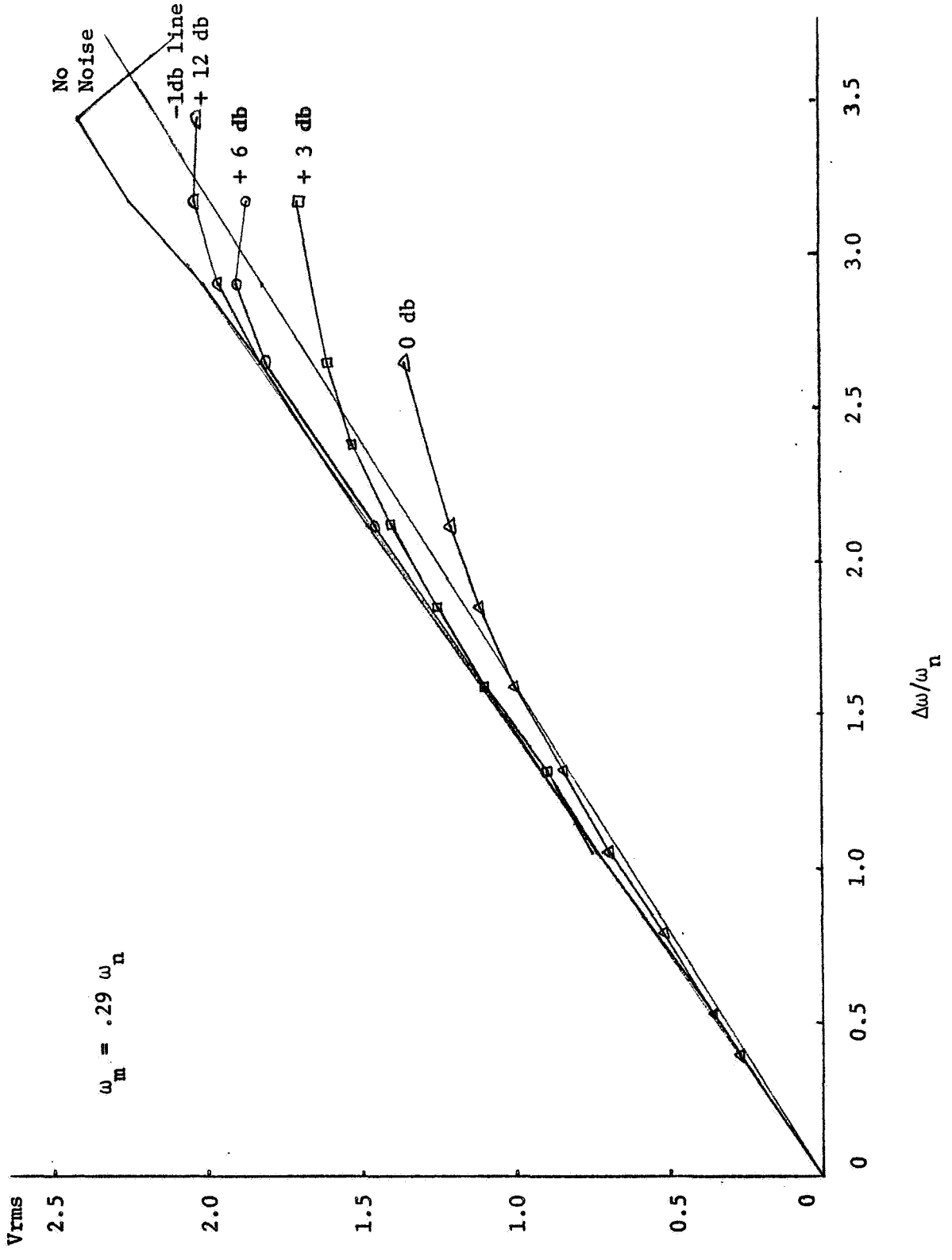

Figure 18

Estimated rms Signal vs. $\Delta\omega/\omega_n$

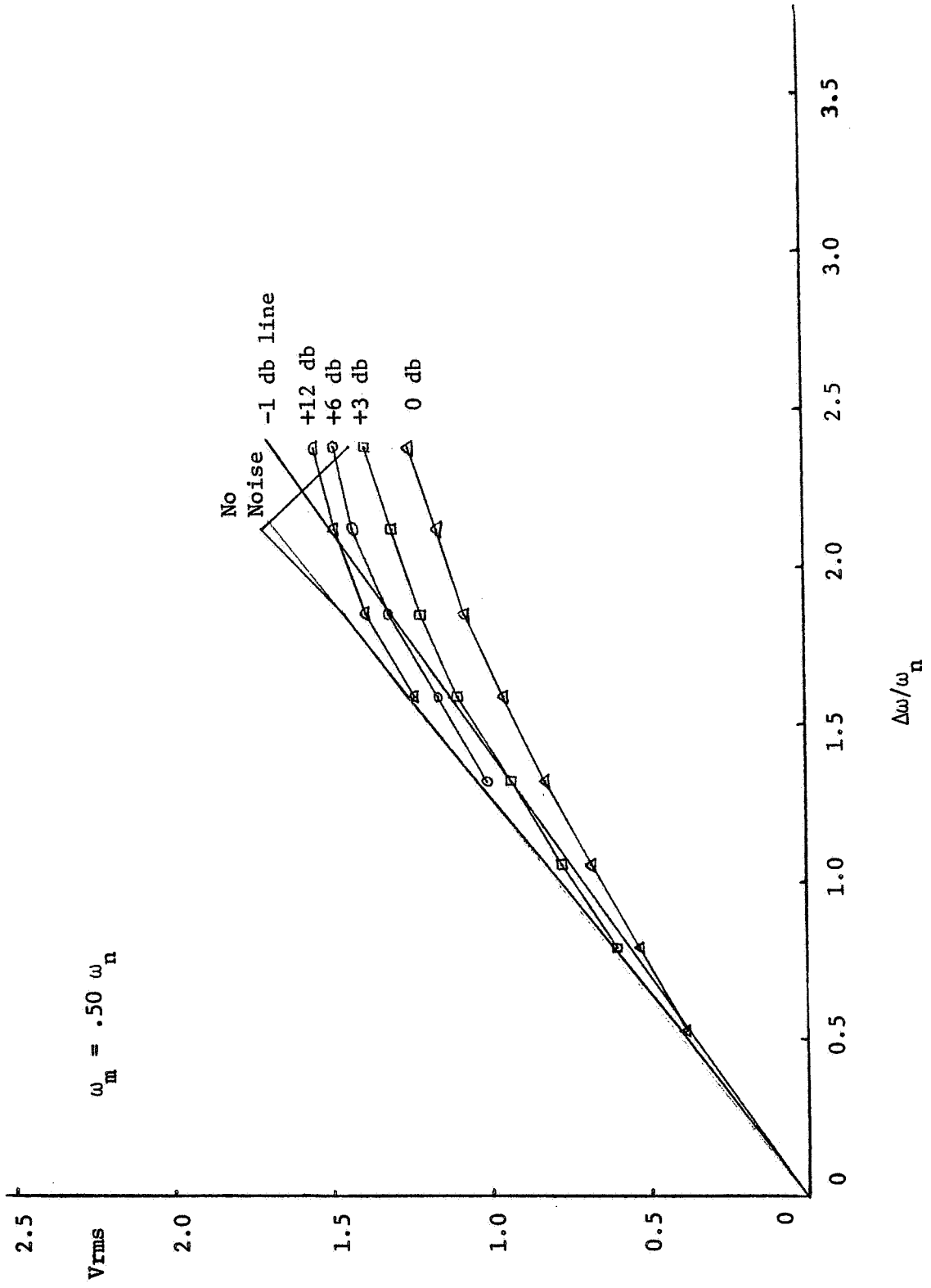

Figure 19

Estimated rms Signal vs. $\Delta\omega/\omega_n$

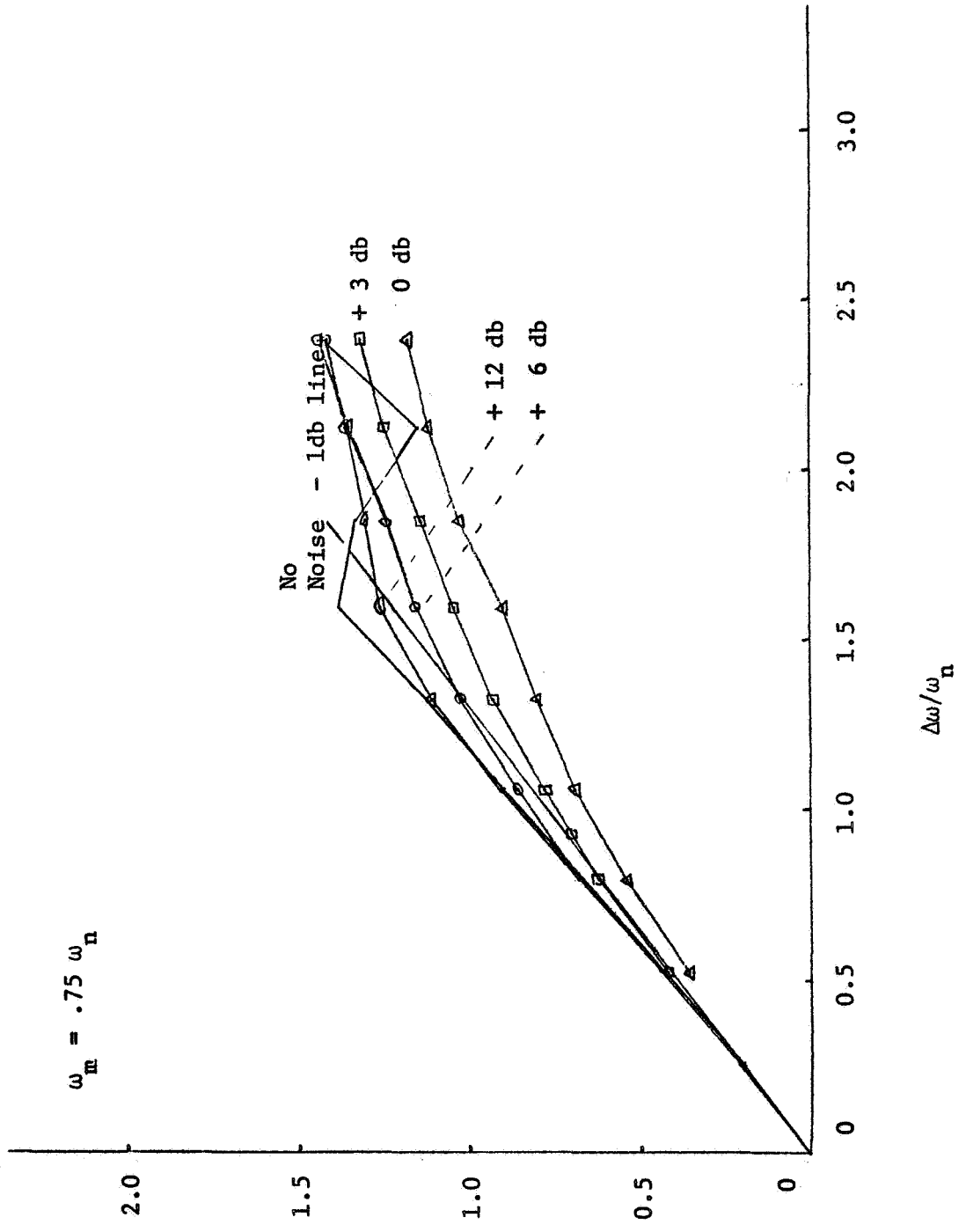

Figure 20

Estimated rms Signal vs. $\Delta\omega/\omega_n$

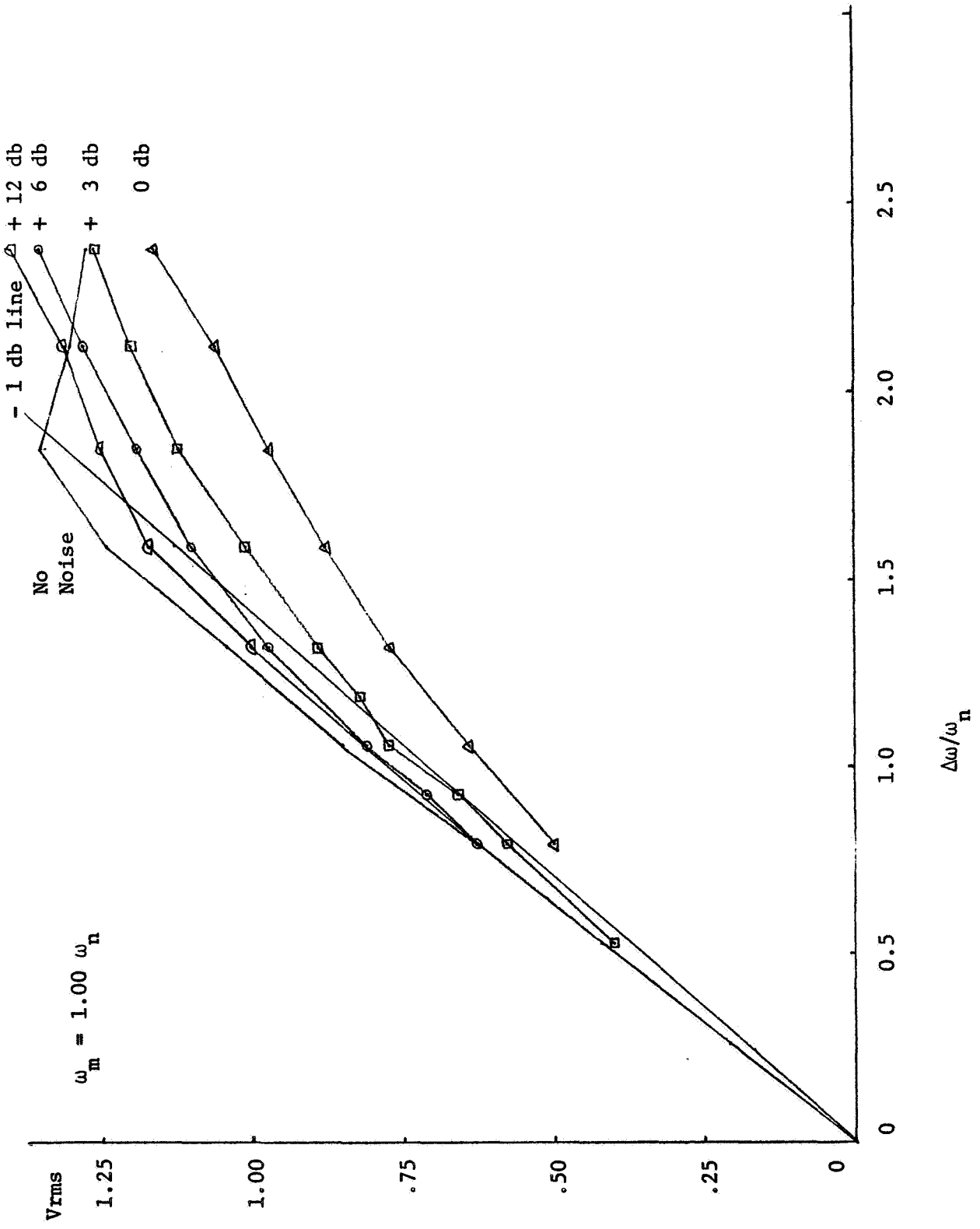

Figure 21

Estimated rms Signal vs. $\Delta\omega/\omega_n$

used until it was decided the results were promising enough to warrant the further coverage of the other frequencies. The graphs display the estimated signal rms voltage, with an arbitrary scale, as a function of $\frac{\Delta\omega}{\omega_n}$ for no noise and +12 db, +6 db, +3 db, and 0 db carrier to noise power ratios. The Vrms scale is left arbitary because the gain of the detector and loop filter in the phase-lock loop determine this level, but are not uniquely determined in a loop with given ω_n and ζ_n. The estimated signal rms voltage $\hat{s}$ is proportional to the square root of the difference between total power out, P_t, and the noise power out with no modulation, P_n.

$$\hat{s} = k \sqrt{P_t - P_n}$$

For the no noise case $P_n = 0$ and for the four noise levels which give +12 db, +6 db, +3 db, and 0 carrier to noise power ratios, P_n varied approximately between the limits indicated by maximum and minimum slopes in Figure 16. This produced no significant problems except for 0 db in the case of $\omega_m = .5, .75$, and $1.00\ \omega_n$. Here the noise power varied between .45 and .50 in the arbitary units chosen for the rms output. At the same time the signal power for $\frac{\Delta\omega}{\omega_n} \leq .5$ was less than .2. Thus the variability in noise power produced sizeable uncertainty in the estimate of signal power in this range of parameters. For this reason the attempt to find accurate points on the 0 db curve in the region $\frac{\Delta\omega}{\omega_n} \leq .5$ was for the most part futile.

One prominent feature in Figures 17 to 21 is the tendency for the estimated signal to very closely follow the no noise signal until a

"threshold" level of $\Delta\omega$ was surpassed, at which time the assumption of constant noise power produced a deviation from this line. Drawn in on each Figure is a straight line which is one db down from the slope determined for the no noise case. The points where estimated signal crossed this line were defined as the thresholds in $\Delta\omega$ beyond which the loop was "significantly" non-linear in its operation. These points are plotted on a $\frac{\Delta\omega}{\omega_n}$ vs $\frac{\omega_m}{\omega_n}$ parameter plane in Figure 22. On this figure the $\frac{\omega m}{\omega_n}$ axis is labeled the -3 db threshold because (referring to Figure 16), it can be seen that the output noise power is one db low from the predicted linear level in the vicinity of -3 db. Vertical bars are used to indicate the uncertainty in the location of the thresholds, due mostly to the interval between applied levels of $\frac{\omega_m}{\omega_n}$, but occasionally due to the low angle between the one db down line and the estimated signal curves or the uncertainty in estimating the signal.

Another feature in Figures 19 to 21 is the difference in behavior of the no noise curve and the noise curves at high $\Delta\omega$. Whereas even the +12 db curve follows the trend established by the other noise curves, the no noise case shows a more drastic drop in signal power beyond the -1 db threshold or the loss of lock level. The presence of small amounts of noise appears to reduce the difference between operating on one side of these thresholds or the other side.

The slope of the no-noise, estimated signal curve varies from one figure to the next in a fully predictable fashion. The estimated signal rms level $\hat{s}$ is obtained by squaring 10e(t), multiplying the result by ten and time averaging, and taking the square root of the result in volts rms.

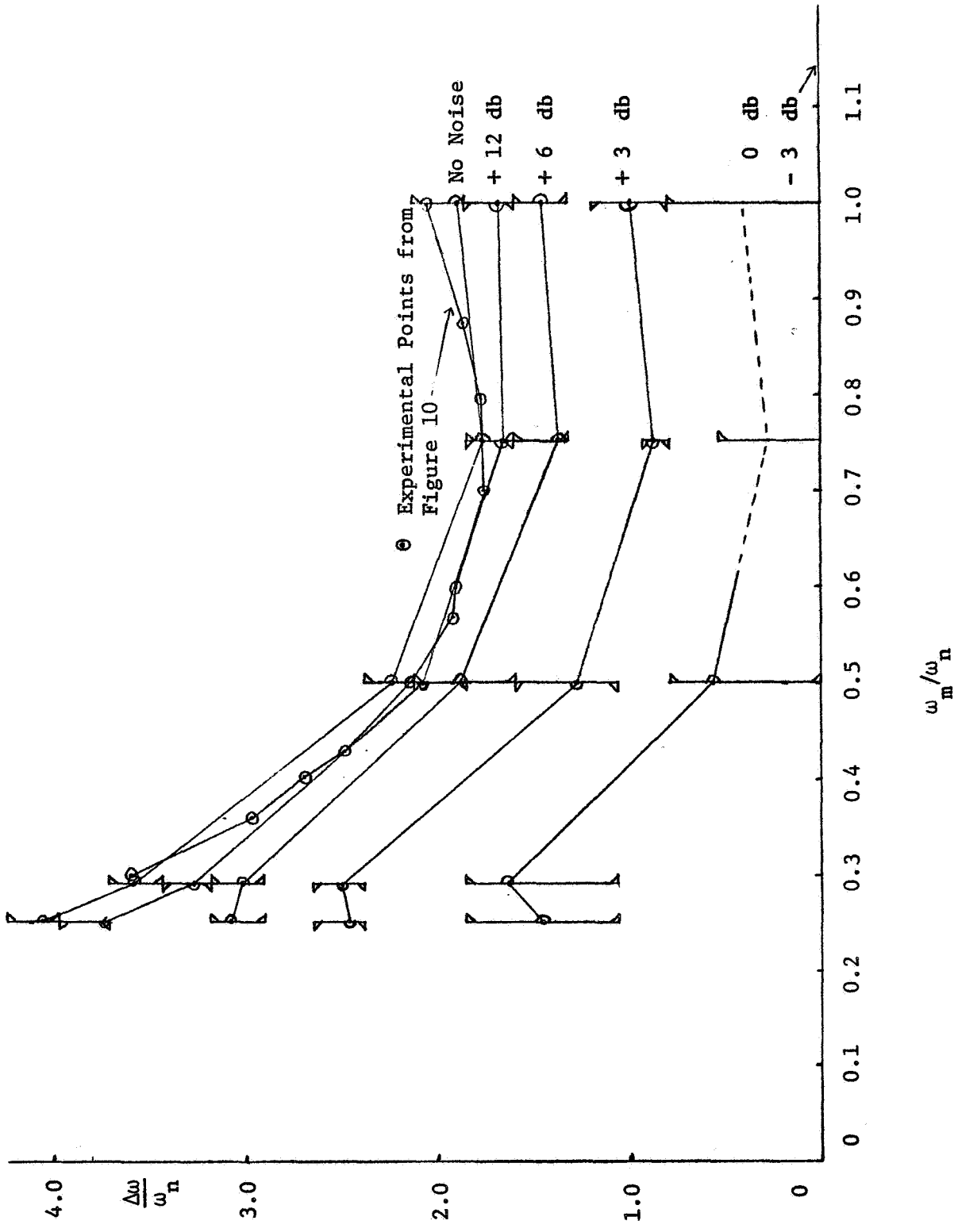

Figure 22

Thresholds in the $\Delta\omega$, ω_m Plane

$$\hat{s} = \overline{[\ 10\ [\ 10e(t)\ ]^2}^{1/2} = 10\sqrt{10}\ \overline{[\ [e(t)]^2]}^{1/2}$$

In the event e(t) is sinusoidal the rms value is just $1/\sqrt{2}$ times the peak value, so

$$\hat{s} = \frac{10\sqrt{10}}{\sqrt{2}}\ e_{max}$$

But

$$e_{max} = \left[\ \frac{d}{dt}\ \frac{\theta_o(t)}{240\pi}\ \right]_{max} = \frac{\frac{d}{dt}\ \theta_{o_{max}}}{240\pi}$$

So

$$\hat{s} = \frac{\sqrt{10}}{24\ \sqrt{2\pi}}\ \left(\frac{d}{dt}\ \theta_o\right)_{max}$$

For a sinusoidal input frequency,

$$\frac{d}{dt}\ \theta_i(t) = \Delta\omega \sin \omega_m t$$

So

$$\frac{1}{\omega_n}\ \left(\frac{d}{dt}\ \theta_i\right)_{max} = \frac{\Delta\omega}{\omega_n}$$

This means

$$\frac{\hat{s}}{\left(\frac{\Delta\omega}{\omega_n}\right)} = \frac{\sqrt{10}\ \ (\dot{\theta}_o)_{max}}{24\ \sqrt{2\pi}\ \frac{1}{\omega_n}\ (\dot{\theta}_i)_{max}} = \frac{\sqrt{10}\omega_n}{24\ \sqrt{2\pi}}\ \left|\ \frac{s\theta_o(s)}{s\theta_i(s)}\ \right|_{s=j\omega_m}$$

The last expression can be evaluated by referring to the linearized transfer function from Chapter I.

$$\frac{\theta_o}{\theta_i} = \frac{K(s + a)}{s^2 + K_s + K_a} = \frac{2\zeta_n \omega_n (s + \frac{\omega_n}{2\zeta_n})}{s^2 + 2\zeta_n \omega_n s + \omega_n^2}$$

$$\left| \frac{\theta_o(j\omega_m)}{\theta_i(j\omega_m)} \right| = \left| \frac{j2\zeta_n \frac{\omega_m}{\omega_n} + 1}{\frac{\omega_m^2}{\omega_n^2} + j2\zeta_n \frac{\omega_m}{\omega_n} + 1} \right|$$

Using $\zeta_n = \frac{1}{\sqrt{2}}$ and $\frac{\omega_m}{\omega_n} = b$ this simplifies to

$$\frac{\theta_o(jb\omega_n)}{\theta_i(jb\omega_n)} = \left[\frac{1 + 2b^2}{(1-b^2)^2 + 2b^2}\right]^{1/2} = \left(\frac{1 + 2b^2}{1 + b^4}\right)^{1/2}$$

Thus

$$\frac{\frac{\hat{s}}{\Delta\omega}}{\omega_n} = \frac{\sqrt{5}\ (21.8)}{24\pi} \left(\frac{1 + 2b^2}{1 + b^4}\right)^{1/2}$$

This formula predicts the slopes of the no-noise curves for different $\frac{\omega_m}{\omega_n}$ values. These are compared in Table 7 with the actual slopes.

Table 7
Demodulation Gains

ω_m/ω_n	$\hat{s}/\Delta\omega/\omega_n$ (Predicted)	(Measured)
.25	.690	.69
.29	.695	.70
.50	.766	.78
.75	.819	.85
1.00	.791	.80

These results are very satisfying, since the staight lines imply that the loop is linear and the prediction here of their slopes implies that the loop obeys the linear transfer function. Thus the total output power is very well predicted from the total input power by the linear transfer function in the case of no noise. Whether this is true also of power at the fundamental of the modulation frequency or not is probably the biggest question raised by these results.

Bibliography

(1) Gardner, Floyd M., Phaselock Techniques. New York, John Wiley and Sons, Inc., c1966. 182p.

(2) Jackson, Albert S., Analog Computation. New York, Toronto, London, McGraw-Hill Book Company, Inc., c1960. 652p.

(3) Carden, F., Lucky, G., and Swinson, G., The Quasi-Stationary and Transient Behavior of Non-Linear Phase-Lock Loops, SWIEEE Record of Technical Program, Dallas, (1967), New York, IEEE, Inc., (1967).

(4) Carden, F., Kelly, L., Hintz, T., The FDM Demodulating Characteristics of Non-Linear Phase-Locked Loops, Proceedings 1968 IEEE National Telemetery Conference, Houston, (1968), New York, IEEE, Inc., (1968) 30-5.

(5) Hancock, Hohn C., An Introduction to the Principles of Communication Theory, New York, Toronto, London, McGraw-Hill Book Company, Inc. c1961. 253p.

(6) Preliminary Instruction Manual Model 603A, Elgenco, Inc., 1550 Euclid Street, Santa Monica, California 90404.